To the Graduate Council:

I am submitting herewith a thesis written by Wendy Faye Lawdermilk entitled "Probabilistic-Mechanistic Simulation and Prediction of Bed-normal Joint Patterns." I have examined the final copy of this thesis for form and content and recommend that it be accepted in partial fulfillment of the requirements for the degree of Master of Science, with a major in Geology.

William M. Dunne

William M. Dunne, Major Professor

Matthew Mauldon

Matthew Mauldon, Major Professor

I have read this thesis and
recommend its acceptance:

Robert D. Hatcher, Jr.

Accepted for the Council:

Vice Provost and Dean of Graduate Studies

PROBABILISTIC-MECHANISTIC SIMULATION AND PREDICTION OF BED-NORMAL JOINT PATTERNS

A Thesis
Presented for the
Master of Science Degree
The University of Tennessee, Knoxville

Wendy Faye Lawdermilk
December, 2001

Copyright © 2001 by Wendy Faye Lawdermilk

All rights reserved

ACKNOWLEDGEMENTS

This research would not have been possible without partial funding from the donors of the Petroleum Research Fund, administered by the ACS; The Geological Society of America; The American Association of Petroleum Geologists; and the Pennsylvania State Survey. I would like to thank my co-advisors, Dr. William M. Dunne (Dept. of Geological Sciences) and Dr. Matthew Mauldon (adjunct Dept. of Geological Sciences & Dept. of Civil and Environmental Engineering, VPI), for their guidance throughout the course of my research. I would also like to thank Dr. Robert D. Hatcher, Jr., (Dept. of Geological Sciences) for his constructive insight. Further, I wish to thank Dr. Terry Engelder (Pennsylvania State University, Geological Sciences) for his hospitality and for his assistance in obtaining field data critical to this research.

I would like to thank my friend, Bruce Rohrbaugh, who not guided me through Visual Basic, but was also kind enough to help me with my fieldwork. To the rest of my friends in the department, thank you for making this an enjoyable experience. And, Dana and Amy, thank you for the stress relief and the laughs.

Last, but certainly not least, I would like to thank my family, especially my parents, for always encouraging and supporting me. To my husband, Mike, thank you for the encouragement and patience.

ABSTRACT

Mechanistic and probabilistic methods have been individually used to characterize and predict joint networks. We feel that combining these two approaches has potential benefit because it overcomes uncertainties associated with mechanics-based models while limiting the probabilistic outcomes with mechanical rules. For this approach, profiles of bed-normal joints were characterized not with fracture trace geometries, but rather with intersection geometries to bedding. T-intersections represent joint termination at bedding, X-intersections represent joints crossing bedding, and E-intersections are those intersections at the sample window edge. Using the intersection counts as input, a new computer program was developed that uses mechanically constrained probabilities to simulate and predict the spatial distribution of bed-normal joints in profiles across bedding. Initially, simulation predictions were compared to ideal joint geometries for one or two lithologies with one or two bed thickness values, and found to match well. Simulation predictions were then compared to joint geometries in five natural profiles from Llantwit Major, Wales, and Huntingdon, PA. Though predictions have variability, they visually resemble the natural profiles and reasonably match the natural values of apparent density, apparent mean tracelength, and intensity. We also considered the issue of extending the methodology to predicting joint networks beyond sample regions by investigating the minimum count of intersections need to produce a representative result. Based on the five natural profiles, which have typical joint geometries, a sample size of about 50-100 intersection counts is sufficient to produce a reasonable prediction of the expected count.

TABLE OF CONTENTS

1. Introduction 1

2. Fracture pattern characteristics 3

2.1. Network characteristics 3

2.2. Intersections versus traces 7

3. Modeling approach 10

3.1. Mechanistic methods 10

3.2. Probabilistic-Mechanistic Approach 13

4. Computer Program Logic 16

4.1. Initiation 18

4.2. Propagation 23

5. Field Data Sets 27

5.1. Llantwit Major 27

5.2. Huntingdon 33

5.3. Network characteristics 34

6. Results 37

6.1. Simulations of ideal cases 37

6.2. Simulation of natural profiles 40

6.3. Comparison of prediction results to natural profiles 46

7. Recommendations for future work 51

8. Conclusions 53

REFERENCES CITED 54

APPENDICES 60

Appendix A. Flow chart describing program decisions 61

VITA 63

LIST OF TABLES

Table 1. Sample window characteristics _____ 17
Table 2. Ideal case profile dimensions and network characteristics _____ 39
Table 3. Lithology parameters and strain for simulations _____ 41
Table 4. Natural profile fracture pattern characteristics and simulation results _____ 35
Table 5. Coefficient of variation for sub-sample intersection counts _____ 48

LIST OF FIGURES

Figure 1. Bed-normal joints in interbedded limestone and mudstone at Llantwit Major, Wales. 4
Figure 2. Geometry of bed-normal joint systems that are (a) bed-contained and (b) not bed-contained (modified from Odling et al., 1999). 5
Figure 3. Bedding profiles with bed-normal joints ornamented for types of joint intersections. 9
Figure 4. Magnitude of bed-parallel tension in a stress shadow (fracture on left), contours are in percentages of the remote tension due to uniform extension. 11
Figure 5. Lengths of open segments (S_i) separated by the stress shadow (shaded areas) for locating a new initiation site. 20
Figure 6. Illustration of assigning probabilities P_i and using a random number R_i to choose an open segment. 22
Figure 7. Inferred propagation behavior at joint-bed intersections for different bedding contact strengths (modified from Cooke & Underwood, 2001). 24
Figure 8. LMP natural profile and simulation results. 28
Figure 9. LM natural profile and simulation results. 29
Figure 10. Hunt1 natural profile and simulation results. 30
Figure 11. Hunt2 natural profile and simulation results. 31
Figure 12. Hunt3 natural profile and simulation results. 32
Figure 13. Ideal case profiles. 38
Figure 14. Graph of % deviation from the expected count for the T-intersections for the five natural profiles and X-intersections for LM, LMP, and Hunt1, versus the normalized expected X and T counts. 49

1. Introduction

This paper presents a quantitative method for simulating and predicting representative fracture patterns in a rock volume from a limited sample size. The method combines existing probabilistic and geomechanical approaches. Specific features of fracture patterns such as fracture orientation, spacing, size, intensity, and termination relationships have been previously investigated (Parker, 1942; Hobbs, 1967; Holst & Foote, 1981; Priest & Hudson, 1981; Hancock, 1985; LaPointe & Hudson, 1985; Verbeek & Grout, 1983; Kulatilake, 1988; Gross & Engelder, 1991; Dershowitz & Herda, 1992; Rives et al., 1992; Barton et al., 1993; Gross et al., 1995; Narr, 1996; Ruf et al., 1998; Mauldon et al., 1999; Bai & Pollard, 2000; Cooke & Underwood, 2001; Mauldon et al. 2001). As recognized by Dershowitz and Einstein (1988), however, the hydraulic and mechanical behavior of fracture patterns are best understood by combining all salient characteristics into a system or network model. The present work uses a combination of density, mean tracelength, and intensity as a network description for bed-normal joints. The new method simulates the spatial distribution of joints and uses these three network characteristics to test predictions.

Approaches to constructing network models include stochastic-geometric characterizations (LaPointe, 1993; Pascal et al., 1997) and geomechanical analyses (e.g. Segall & Pollard, 1983; Olson & Pollard, 1989). Stochastic descriptions of joint patterns replicate geometric characteristics of fracture networks via probability distributions such as Poissonian or fractal (e.g., LaPointe, 1993). In contrast, mechanical analyses incorporate boundary conditions, material behavior, and state parameters to predict a

joint network (e.g., Pollard & Segall, 1987). The basic limitation of a statistical approach is that it applies a quantitative characterization to attributes without understanding their origin. In contrast, insufficient information about forces, material behavior, and initial state prevents mechanical analyses from accurately predicting fracture patterns. Also, when investigating joint development in inhomogeneous media with pre-existing discontinuities, such as a profile across bedding, these analyses tend to consider a very limited area due to computational difficulties rather than an area representative of a joint network (e.g. Cooke & Underwood, 2001; Engelder & Peacock, 2001; Bai & Pollard, 2000). Due to these limitations, I blend the two approaches in an attempt to minimize their weaknesses. A combination of these two approaches may be appropriate because (1) initial and boundary conditions for a mechanical analysis are not predicted uniquely from a final geometry, creating uncertainty; and (2) statistical methods are ideally suited to dealing with uncertainties because they are based in probabilistic analysis. The approach also provides investigators with a means of quickly testing whether their primary mechanical controls are yielding the anticipated effect. This new approach will be applied to the common case of bed-normal joints in sedimentary rocks, which has been the focus of numerous geometric and mechanical studies (e.g., Hobbs, 1967; Narr & Lerche, 1984; Olson & Pollard, 1989; Helgeson & Aydin, 1991; Gross et al., 1995; Becker & Gross, 1996; Narr, 1996; Pascal et al., 1997; Ruf et al., 1998; Bai & Pollard, 2000).

2. Fracture pattern characteristics

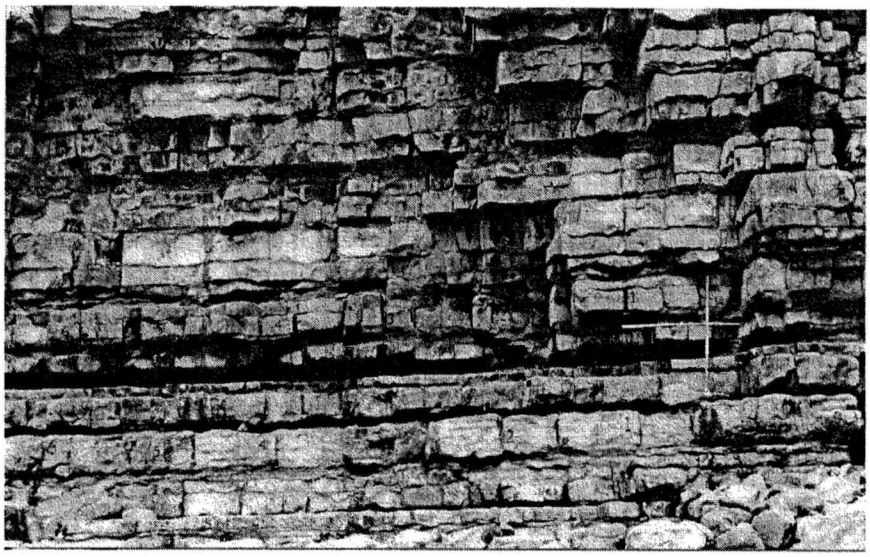
2.1. Network characteristics

Before explaining the simulation approach, the observational framework and salient network characteristics need to be established. A single bed-normal joint set in sedimentary rocks forms a simple common fracture network (Helgeson & Aydin, 1991; Gross et al., 1995; Becker & Gross, 1996; Pascal et al., 1997; Gillespie et al., 2001). Data about these joint patterns are typically gathered from rock exposures such as natural pavements, roadcuts, cliffs, tunnels, or boreholes. These exposures can be sampled by constructing trace maps, or using straight or circular scanlines (e.g. Terzaghi, 1965; Hudson & LaPointe, 1985; Priest, 1993; Wu & Pollard, 1995; Becker & Gross, 1996; Narr, 1996; Gillespie et al., 2001; Mauldon et al., 2001).

A typical characteristic for a single set of bed-normal joints is that fracture dimension normal to bedding is much smaller than parallel to bedding (Fig. 1). This size difference may be one to three orders of magnitude. Since joints are laterally extensive parallel to bedding, we can analyze their development in the two-dimensional plane normal to both the joints and the beds. In this two-dimensional profile, the bed boundaries and fractures are both represented by traces.

Connectivity and termination relationships for a single set of bed-normal joints, are with bedding and not each other (Fig. 2). Therefore, the abundance and size of joint traces are of primary interest when characterizing the fracture network, which in this study, are described by intensity, density and mean tracelength. Based on earlier work of Dershowitz and Herda (1992), a unified system of fracture abundance measures has

a)



0 1 m

b)



Fig. 1 Bed-normal joints in interbedded limestone and mudstone Llantwit Major, Wales. (a) Cliff face. (b) Bedding pavement beneath the cliff face, arrow length of 1 m refers to foreground, illustrating that the older master joints are much longer parallel to bedding than perpendicular to bedding.

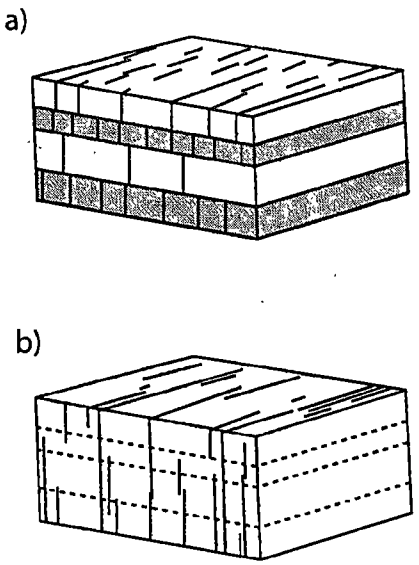


Fig. 2 Geometry of bed-normal joint systems that are (a) bed-contained and (b) not bed-contained (modified from Odling et al., 1999)

recently been proposed by Mauldon and Dershowitz, 2000. In that system, abundance measures are identified by a capital P with two subscripts. The first subscript denotes the dimension of the measurement region; the second denotes the dimension of the attribute being measured. For example, two-dimensional intensity is fracture length (1-d) per unit area of sampling plane (2-d) and is denoted P_{21}. This notation will be used in the present study to denote intensities and densities.

Fracture intensity (P_{21}) in two dimensions is essentially the product of density and mean tracelength, and as such incorporates both fracture size and number. For the two-dimensional case, intensity is measured as total fracture length in the sample divided by sample area. In the one-dimensional case of a scanline along a bed, intensity (P_{10}) is the inverse of spacing, which has been widely investigated for the case of bed-normal joints (e.g., Price, 1966; Becker & Gross, 1996; Pascal et al., 1997; Ruf et al., 1998; Bai & Pollard, 1999). Intensity rather than spacing is used for characterization because it is scale independent, and it links density and mean tracelength, providing a consistent set of fracture characteristics (Mauldon et al., 2001).

Two-dimensional fracture density (P_{20}) is the number of trace centers per unit area (Mauldon, 1998). Yet, because full fracture tracelengths are not always visible in the sample window, an effect known as censoring, not all trace centers may be identified. Commonly the apparent density, which is the total number of partial and whole traces in the outcrop window divided by the area, is often determined. This scale-dependent parameter (apparent density ρ') yields an overestimate of true trace density (Mauldon et al., 2001).

Mean tracelength (μ) is the average length of all fracture traces on a plane of specified orientation. Given the competing sampling biases of censoring that curtails traces and length bias that favors the sampling of longer traces, determination of μ can be problematic (Baecher & Einstein, 1977). Often apparent mean tracelength (μ'), the average length of all visible traces and portions thereof, is measured, but this tends to underestimate true mean tracelength (Baecher and Einstein, 1977, Mauldon, 1998).

2.2. Intersections versus traces

A major difficulty for characterizing fracture network patterns is the limited exposure of joint traces. If complete exposure were available, full tracelengths could be measured and trace centers could be identified so that true mean tracelength and density could be determined for a fracture network. Data quality about fracture pattern characteristics decreases as the sample size for a population of fracture traces decreases and the effects of sampling bias increase (Mauldon et al., 2001; Rohrbaugh et al., in review). This issue is exacerbated for boreholes, where hole diameters are typically much smaller than fracture size (Narr & Lerche, 1984; Narr, 1996), and censoring is a significant bias.

Given the sampling biases associated with characterizing a population of traces, we applied a new method that uses points rather than lines in an attempt to reduce the bias effects. The points are located at the intersections between joints and bedding surfaces. The intersection types are:

T-intersection: a joint terminates at a bedding surface

X-intersection: a joint crosses a bedding surface

E-intersection: a joint trace intersecting the edge of the sampling window (Fig. 3a).

Counting the three types of intersections is simple (Fig. 3), even with limited exposure. The counts quickly illustrate whether bed-normal joints are contained or not contained, because counts dominated by T-intersections are indicative of bed containment (Fig. 3b) whereas large X-intersection counts are indicative of joints not bed contained (Fig. 3c).

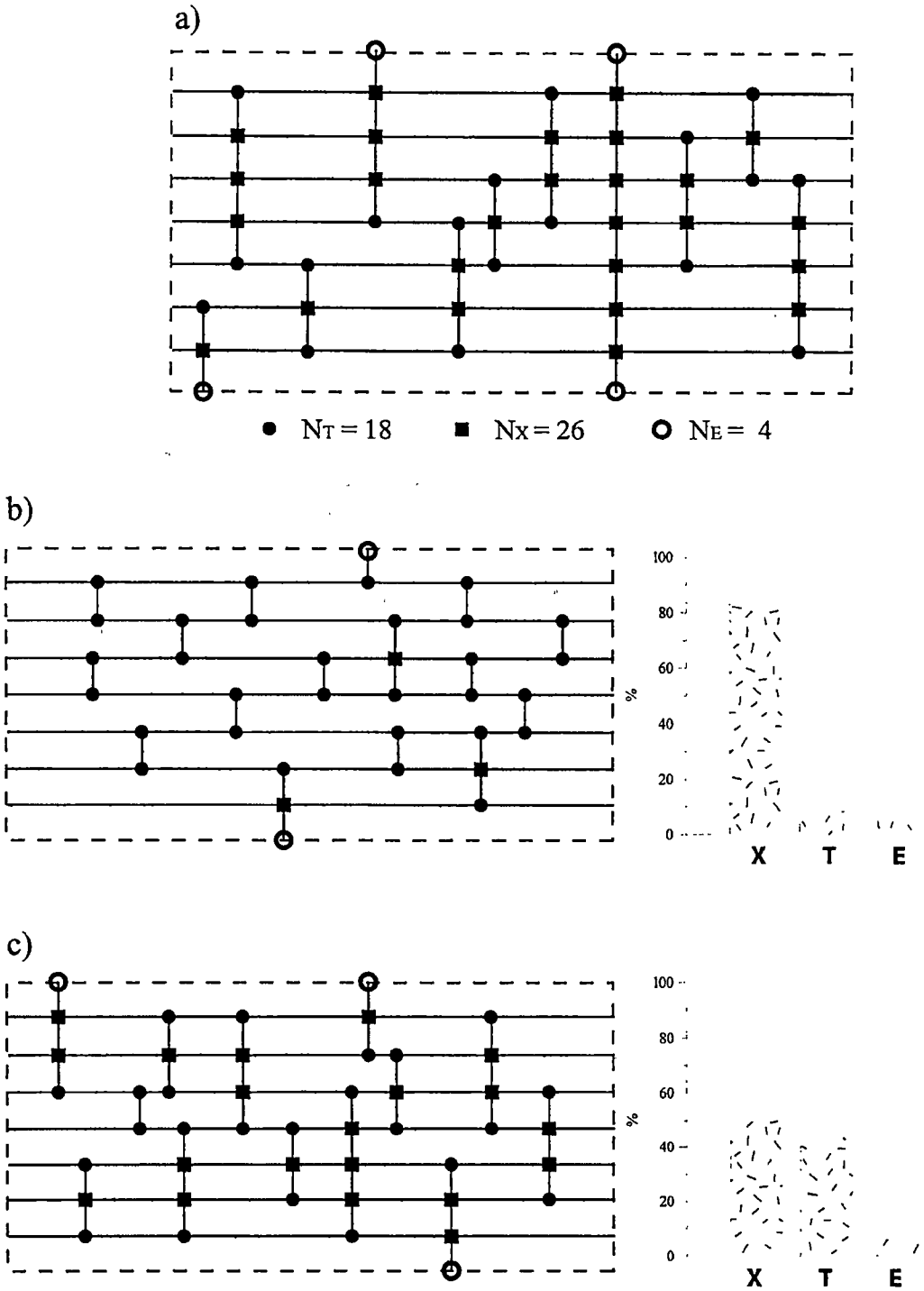


Fig. 3 Bedding profiles with bed-normal joints ornamented for types of joint intersections. a) General case to demonstrate intersection types. b) Dominance of T-intersections for bed-contained joints. c) Abundance of X and T intersections for joints corossing bedding surfaces.

3. Modeling approach

3.1. Mechanistic methods

Mechanics-based simulation of joints commonly uses linear elastic material properties, boundary conditions, and initial state conditions to predict the formation and resultant geometry of structures. In the case of bed-normal joints, parameters such as in situ stress, confining pressure, fluid pressure, strain rate, Young's modulus and fracture toughness influence fracture development and geometry (Segall, 1983; Segall & Pollard, 1987; Gross et al., 1995; Engelder & Fischer, 1996; Olson, 1997). For the specific case of fractures formed by a remote extensional strain, the applied strain produces a stress in the rock volume as a function of elastic properties (Hobbs, 1967; Gross et al., 1995; Bai & Pollard, 2000).

An example of a mechanics-based forward model for investigating fracture geometry is Gross et al., (1995), who use a two-dimensional finite element model to characterize the stresses adjacent to a fracture. Their study demonstrates that stress is zero adjacent to the joint and increases to the remote stress at an infinite distance from the fracture (Fig. 4) (Gross et al., 1995). The study shows that bed thickness, elastic moduli, extensional strain, and flaw size and placement all influence joint spacing. In another example, Olson (1997) focuses on mechanical analysis to develop his model exploring subcritical crack growth. By maintaining the same boundary conditions and material properties he was able to explore the effects of bed thickness on fracture patterns. The model predicts that thicker beds increase average joint spacing, increase joint clustering, decrease fracture density, and generate more fracture-path curving (Olson, 1997).

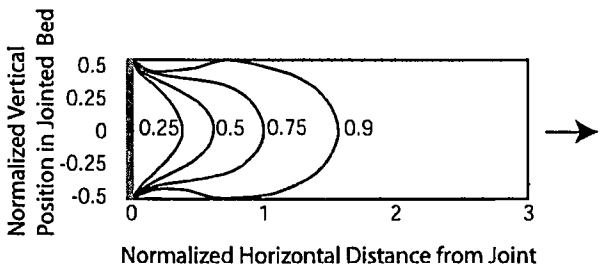


Fig. 4 Magnitude of bed-parallel tension in a stress shadow (fracture on left), contours are in percentages of the remote tension due to uniform extension. The layer was modeled with a Young's modulus of 17.5 GPa and bounding mudstones (modified from Gross et al., 1995).

Mechanics-based modeling of joint development involves a large number of parameters related to material properties, initial state conditions, and several possible processes that can exert a strong influence on fracture growth. Different combinations of material properties and loading conditions can lead to similar or identical fracture patterns. Thus, more than one possible explanation exists for the same phenomenon and rocks may not contain features that differentiate between the choices, which is a difficulty characteristic of understanding geologic processes. For example, Olson & Pollard (1989) demonstrated a method for inferring differential stress based on the degree of tip curvature of en echelon joints as a function of the relative magnitudes of remote and crack-tip stress. Yet, curvature may also be influenced by sub-critical fracture growth and fracture roughness (Renshaw & Pollard, 1994). Thus, straight joints may develop because of a large differential stress, sub-critical fracture growth by decreasing the necessary driving stress, or fracture surface roughness by limiting the magnitude of shear displacement discontinuity that can be accommodated, but natural joints lack features to distinguish between the causes.

Another source of uncertainty in mechanical modeling is limited knowledge of initial geometric conditions that lead to joint propagation in nature. For example, many mechanical models assume initial size and spatial distributions for the pre-existing flaws that serve as loci for joint initiation (e.g., Segall, 1984; Rives et al., 1992; Gross et al., 1995). The size of preexisting flaws influences the stress necessary for joints to initiate, since larger flaws require less stress to propagate into joints (Segall, 1983; McConaughy & Engelder, 2001; Weinberger, 2001). Spatially, joints initiating near bed edges will be

more closely spaced than if initiated in bed centers (Gross et al., 1995; Bai & Pollard, 2000b). Despite being aware of conditions where flaw distribution favors joint formation, little is actually known about flaw size and spatial distributions in nature.

3.2. Probabilistic-Mechanistic Approach

Given the uncertainties involved in defining parameters for a realistic mechanical model and in verifying the results with respect to natural systems, we believe that it is useful to incorporate a probabilistic aspect to the analysis to deal with these uncertainties. Rock fracture patterns have been studied extensively using probabilistic methods since the 1970's (Baecher & Einstein, 1977; Cruden, 1977; Warburton, 1980; Pahl, 1981; Hudson & Priest, 1983; LaPointe & Hudson, 1985; Dershowitz & Einstein, 1988; Kulatilake, 1988; Dershowitz & Herda, 1992; LaPointe, 1993; Priest, 1993; Mauldon, 1994; Odling, 1997; Mauldon, 1998; Zhang & Einstein, 1998). The starting point for this viewpoint is the recognition that fracture location within a layer, as observed in thin section, borehole, outcrop, or geologic map, is a snapshot of a random process, akin to a photograph of cars on the freeway. In this context, process does not refer to the mechanical and geologic processes that led to fracture formation, but to the overall spatial pattern of which the observed fractures (or cars) are a sample. Random in this sense does not mean arbitrary or unconstrained, but instead means that a fracture characteristic such as location can be usefully viewed as being governed by probability laws. Such probability laws may take on any of a variety of forms, and can themselves depend on geologic or other factors at any desired level of detail.

To illustrate, hypothetical probability distributions for bed-normal fracture spacing in sedimentary rocks might include the following: constant spacing equal to bed thickness (Bai & Pollard, 2000a), lognormal (Rives et al., 1992), negative exponential (Priest & Hudson, 1981), or power law / fractal (Barton, 1995). Such distributions can be modified according to geologic or mechanistic principles by conditioning on pertinent information about material parameters, local or remote stress, fractures in the adjacent bed(s) and so on, as long as they meet the requirements of the three axioms of probability theory (Ang & Tang, 1975). Thus, probabilistic models are very flexible and can be tied in natural ways to the geologic setting and to the mechanics perceived to govern fracture formation.

In this study, simple mechanistic rules are linked to a simple probabilistic decision model of fracture initiation and propagation. Mechanistic rules are used to preclude violations of mechanical principles. For example, requiring the driving stress to exceed a critical value precludes fracture initiation inside stress shadows. Thus, fractures form with spacings typical of natural examples where stress shadows likely operated, which would not be the case for an unrestricted Poissonian fracture distribution. Another example involves termination and propagation of fractures at bedding boundaries. Mechanistic rules about interface properties are used to influence model decisions about propagation of fractures into the next bed, reducing the need to infer overall fracture geometry from a necessarily limited sample. Furthermore, mechanical rules also eliminate the need to use a predetermined distributional form for network parameters.

Combining probabilistic modeling with mechanical constraints can minimize the weaknesses of each approach, while exploiting their strengths. A probabilistic approach can deal with aspects of an analysis where uncertainty exists about inputs for mechanical calculations. Use of probabilities allows for a decision when mechanical rules do not offer a unique answer. For example, assigning probabilities provides a way to determine the location of a new fracture when there are multiple locations that meet the initiation criteria. The result of combining the two approaches should be a predictor of representative final geometry, from a limited sample, based on mechanical principles.

4. Computer Program Logic

The approach uses a Visual Basic™ computer program to simulate fracture networks based on probabilities constrained by geomechanical rules. The main inputs are lithological properties, bedding parameters, which are the thickness and lithology of each bed, and the (T, X, E) intersection counts normalized by outcrop area (e.g. Table 1). Once bedding geometry is defined, fractures are initiated and propagated in a series of iterative steps. The decision processes of the program are outlined in the flow chart of Appendix A.

In each loop, the program determines if the stopping parameters are met, and if not, then proceeds to the next determination of initiation or propagation. The decision to initiate a new joint or propagate an existing joint is determined with a probability based on the normalized fracture-bedding intersection counts. Since a new T-intersection requires a new fracture, the probability of initiation is set proportional to the difference between the current normalized N_T count in the simulation and the target normalized N_T. Every X-intersection represents a fracture that propagated across a layer boundary, so the probability assigned to the decision to propagate is proportional to the difference between the current normalized N_X count and the target normalized N_X. The probability of either action goes to zero when the current normalized intersection count equals the target normalized intersection count, and when both targets, X- and T- normalized counts, are reached. Then, the program stops.

Table 1
Sample window characteristics

	LMP	LM	Hunt1	Hunt2	Hunt3
Window Height (m)	2.51	1.77	3.62	4.00	3.99
Window Length (m)	11.16	9.00	12.20	8.20	7.20
Window Area (m^2)	28.01	15.89	44.16	32.80	28.73
Number of beds	13	13	23	21	12
T-intersections	270 (0)	422 (74)	392 (12)	216 (0)	157 (11)
X-intersections	326 (0)	94 (4)	65 (0)	1 (0)	3 (0)
E-intersections	82	78	12	0	11

The counts in parentheses represent known E-intersection counts, for example profile Hunt3 has 11 E-intersections, however these are actually known to be T-intersections s 11 appears in parentheses for T-intersections.

4.1. Initiation

When the decision is made to initiate a new joint, the next step is to determine the fracture location. This analysis assumes a uniform initial flaw distribution, so that all locations can act as the nuclei for fracture growth. However, an initial flaw will propagate and form a fracture only if the stress intensity at the crack tip exceeds the fracture toughness (K_{Ic}) of the material (Gross et al., 1995). The critical stress (σ_f) for crack propagation can be expressed by:

$$\sigma_f = \frac{K_{Ic}}{\sqrt{\pi c}} \qquad (1)$$

where c is the crack half-length. For joint initiation, the crack length is the initial flaw size, so the longer the initial flaws, the less stress necessary for joint initiation. For this analysis, driving stress (σ) is proportional to the uniform remote extensional strain (ε), according to the equality:

$$\sigma = E * \varepsilon \qquad (2)$$

where E is Young's modulus (Engelder, 1993). Given the same strain, lithologies with greater Young's moduli will experience greater stress than those with lower Young's moduli. If the resulting stress in a particular lithology exceeds the critical fracture stress (σ_f), fractures can initiate in that lithology. For bed-contained, bed-normal joints, spacing is often thought to be proportional to bed thickness (Price, 1966) because spacing is partly controlled by the size of the fracture stress shadows (Fig. 4), which are areas of reduced stress immediately adjacent to an existing fracture (Hobbs, 1967). This stress

reduction exists because tensile stress cannot be transmitted across an open fracture face. The extent of a stress shadow is dependent on the linear elastic material properties, fluid pressure, and remote stress (Gross et al., 1995). Field studies have found joint spacing to layer thickness ratios ranging from less than 0.1 to 10, with the most common values between 0.3 and 1.2 (Bai & Pollard, 2000). It has also been demonstrated that at a critical spacing-thickness ratio, typically near 1, normal stress acting perpendicular to joints becomes compressive, preventing fracture formation (Bai & Pollard, 2000). Thus, networks with ratios between 0.8 and 1.2 are at or near saturation, which is a state where stress shadows prevent joint initiation (Bai & Pollard, 2000). Because many researchers have reported a spacing-thickness ratio near unity (e.g. Huang & Angelier, 1989; Wu & Pollard, 1995; Ruf et al., 1998) and saturated ratios center on this value, the default program value for the shadow size in proportion to bed thickness is 1 (Fig. 5), but the value may be varied by lithology or set to zero. Also, for the case of joints not bed-contained, the size of the stress shadow, if operative, is set equal to the fracture height, since it can no longer be related to bed thickness. For initiation, the stress shadow is viewed as a finite zone within which new fractures cannot form, rather than as a contained region of reduced stress (as in Fig. 4).

The simulation window is divided into open segments (Fig. 6) which lack stress shadows, where new fractures can initiate. In this study, it was assumed that the chance of a joint initiating from a flaw in a given segment is proportional to the segment length, everything else being equal. So, each segment is weighted according to its length (S), but not according to thickness.

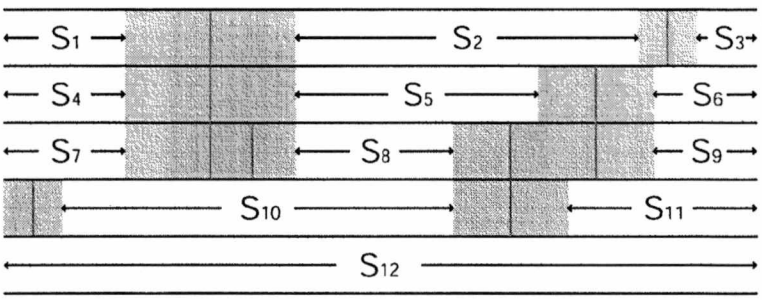


Fig. 5 Lengths of open segments (Si) seperated by the stress shadow (shaded area) for locating a new initiation site.

Another significant factor is the segment lithology. Fracture toughness of the lithology influences fracture initiation by determining the necessary stress for crack propagation, while Young's modulus controls the stress experienced for a given remote strain. The default flaw size for the program was chosen as 0.005 m, but this parameter may also be varied by lithology. Gross et al., (1995) studied the effect of initial flaw size on fracture spacing. An initial flaw size of 0.005 m produced a spacing ratio of 0.82 while an initial flaw size of 0.003 m produced a spacing ratio of 1.25. McConaughy & Engelder (2001) studied fracture initiation points in siltstone beds of the Ithaca Formation and found that thin shale laminae (<0.005 m) served as initiation points, showing that natural joints can form from this size flaw. To incorporate effects of segment length and lithology we define the probability of each segment by:

$$p(\text{init})_i = S_i * \frac{1}{K_{Ic_i}} * \sqrt{\pi c_i} * E_i \qquad (3)$$

where S_i, K_{Ic_i}, c_i, and E_i are the segment length, fracture toughness, crack half-length, and Young's modulus, respectively, associated with the i^{th} segment. Then the probability that the i^{th} segment contains the new joint, given the decision to initiate, is given by:

$$\text{Prob(initiation in segment i | initiation)} = \frac{p(\text{init})_i}{\sum_{i=1}^{n} p(\text{init})_i} \qquad (4)$$

An open segment is then selected using a random number (Fig. 6). Once a segment is chosen, the fracture location with the segment is assigned a uniform distribution, so a

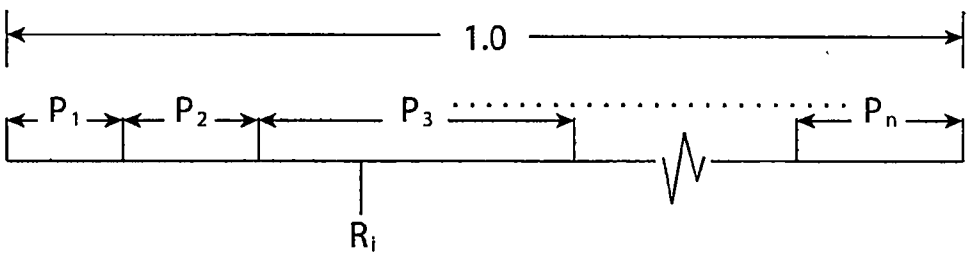


Fig. 6 Illustration of assigning probabilities Pi and using a random number Ri to choose an open segment.

second random number is used to choose a location within the segment. For each subsequent fracture initiation, the same process is followed, redefining the segments each time according to existing fractures and their shadows. The program also allows the user to "turn off" stress shadows for analysis of data sets with closely spaced fractures. This choice may be necessary for joints that are primarily not contained and are too closely spaced for stress shadows to either have been operative or to have controlled spacing. For instance, vein fill at the time of joint formation, may preclude stress reductions, since it allows stress transmission between the joint faces.

4.2. Propagation

For the case of joint propagation, each end of a fracture is considered separately, because interfaces between layers of different lithologies influence joint propagation in sedimentary rocks (Helgeson and Aydin, 1991; Cooke and Underwood, 2001). Also variation in bedding contact strength affects the ability of fractures to propagate across bedding boundaries (Cooke & Underwood, 2001). Strong contacts allow fractures to propagate, while weak interfaces result in fracture termination, and interfaces of moderate strength lead to either fracture termination or fracture step-over (Fig. 7). Since weak bedding contacts prevent propagation, the user is allowed to designate if fractures can or cannot propagate into certain lithologies. Stress can also be communicated across thin inhibiting layers and can initiate a new fracture in the next bed adjacent to the inhibiting layer, resulting in a composite joint (Helgeson & Aydin, 1991). However, shale layers as thin as 1 cm can limit stress communication and layers less than 40 cm

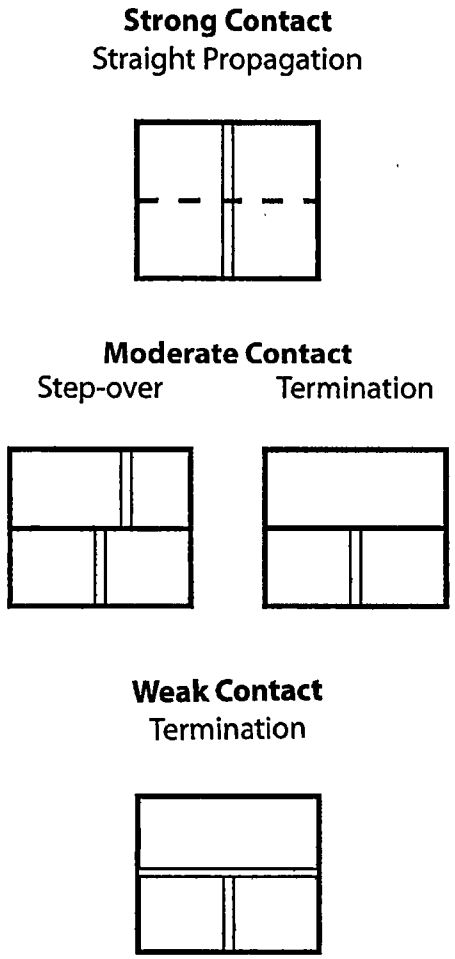


Fig. 7 Inferred propagation behavior at joint-bed intersections for different bedding contact strengths (modified from Cooke & Underwood, 2001).

thick can mechanically isolate adjacent beds (McConaughy & Engelder, 2001). Since mudstones in this study range from 1 cm to 180 cm in thickness, the analysis does not consider composite joints.

Fracture length influences propagation because longer joints require less stress to propagate than shorter joints. Lithology also influences propagation, through fracture toughness (K_{Ic}) and Young's modulus (E), in the same manner it influences initiation. Therefore each fracture end i that was not eliminated by weak interfaces is weighted by the square root of fracture half-length (c) and the lithology that the joint will penetrate, by:

$$p(prop)_i = \sqrt{\pi c_i} * \frac{1}{K_{Ic_j}} * E_j \qquad (5)$$

where subscript i refers to the fracture and subscript j refers to the adjacent bed. Then, given the decision to propagate, the probability of the i^{th} end propagating is given by:

$$\text{Prob(propagation from end i | propagation)} = \frac{p(prop)_i}{\sum_{i=1}^{m} p(prop)_i} \qquad (6)$$

A random number is used to choose a fracture end (Fig. 6). For that end, driving stress is compared to critical stress to determine if propagation occurs. The local stress is modified by the presence of a stress shadow. While stress shadows may have complex configurations, to simplify the model, shadows are modeled as zero stress at the fracture face with stress increasing linearly to the magnitude of the remote stress at a distance equal to fracture height. If overlapping stress shadows exist where the fracture will

propagate, the cumulative reduction is considered. If this local driving stress equals or exceeds the fracture stress, the fracture propagates.

5. Field Data Sets

Five natural profiles are used in this research (Fig. 8a-12a). Two profiles, including one from previous work (Pascal et al., 1997), are from Llantwit Major, Wales, in a sequence of interbedded limestone and mudstone. Three new profiles are from Huntingdon, Pennsylvania, USA, in a sequence of interbedded sandstone, siltstone and mudstone. The profiles represent typical geometries for bed-normal joints in sedimentary rocks with different interbedded lithologies and a range of termination relationships.

5.1. Llantwit Major

The first data set (LMP, Fig. 8a), reproduced from Pascal et al. (1997), is from a cliff containing a bed-normal set of master joints (striking N170°) cutting horizontally layered rocks of the Jurassic Porthkerry Formation at Llantwit Major, Wales (Pascal et al., 1997). The formation consists of micritic limestone beds that are decimeters thick and mudstone interbeds that are centimeters thick. The profile is comprised of both bed-contained joints and joints that cross multiple beds. A new second profile (LM, Fig. 9a) was collected for this study in a nearby cliff face. The joints of this profile are mostly bed-contained. Llantwit Major is the site of a previously published two-dimensional probabilistic model for bed-normal joints in interbedded sedimentary rocks (Pascal et al., 1997). Their analysis used as input the total number of joints visible in the outcrop, the number of limestone beds, the number of joints in each limestone bed, the number of joints common to a limestone bed and the closest limestone bed below it, the thickness of each bed, and the outcrop length. Although the Pascal et al. (1997) analysis did produce a

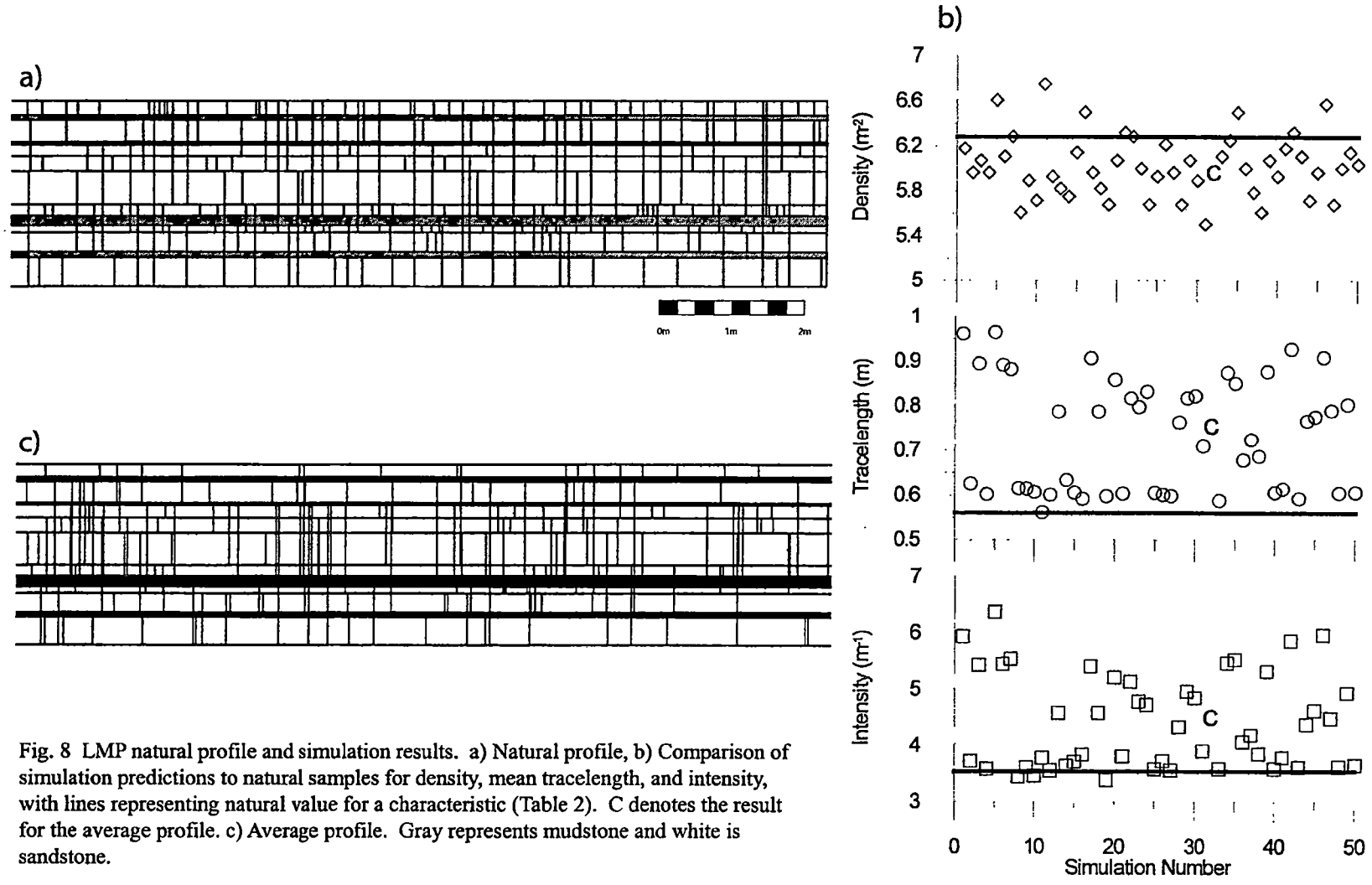


Fig. 8 LMP natural profile and simulation results. a) Natural profile, b) Comparison of simulation predictions to natural samples for density, mean tracelength, and intensity, with lines representing natural value for a characteristic (Table 2). C denotes the result for the average profile. c) Average profile. Gray represents mudstone and white is sandstone.

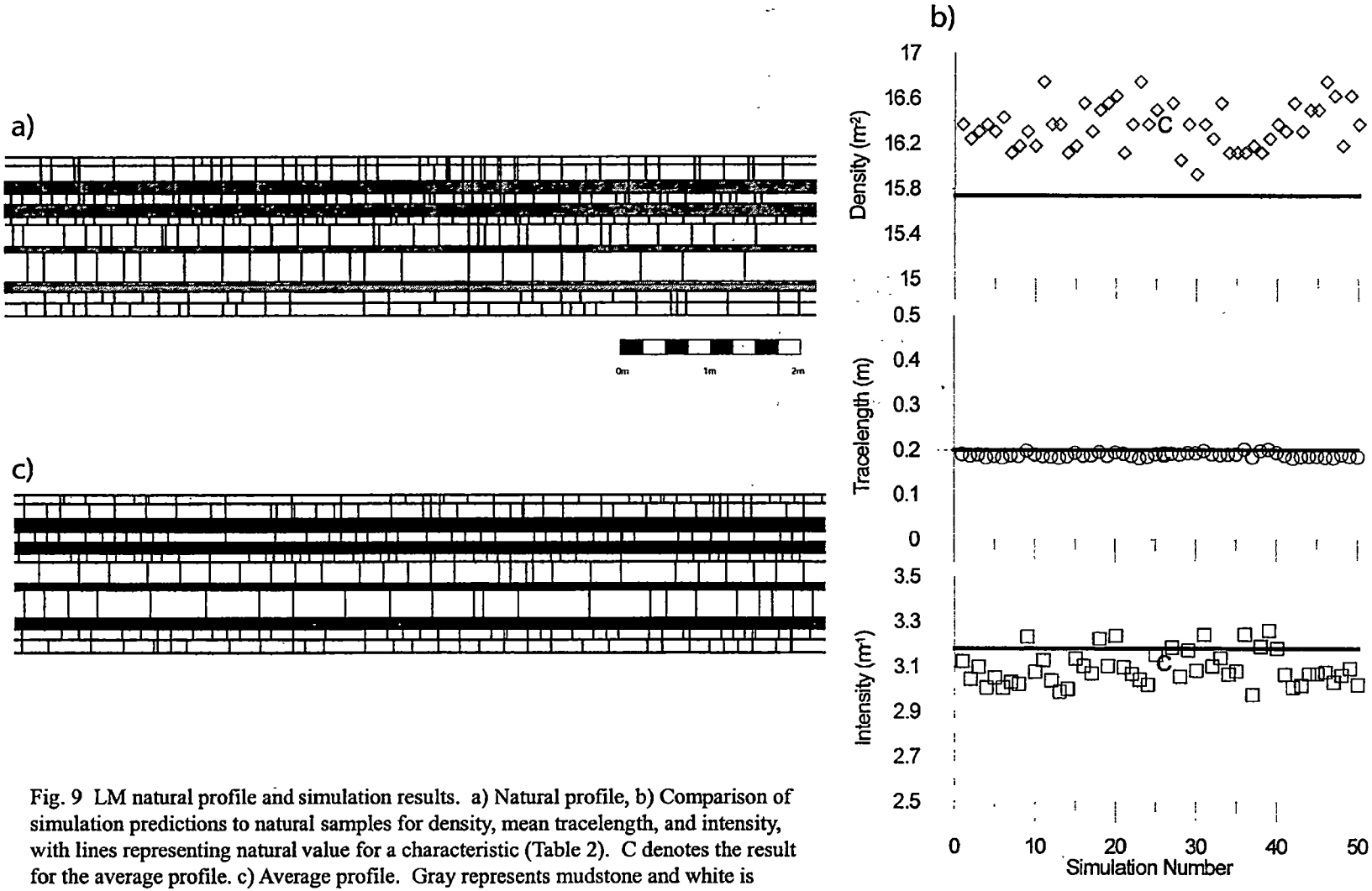


Fig. 9 LM natural profile and simulation results. a) Natural profile, b) Comparison of simulation predictions to natural samples for density, mean tracelength, and intensity, with lines representing natural value for a characteristic (Table 2). C denotes the result for the average profile. c) Average profile. Gray represents mudstone and white is sandstone.

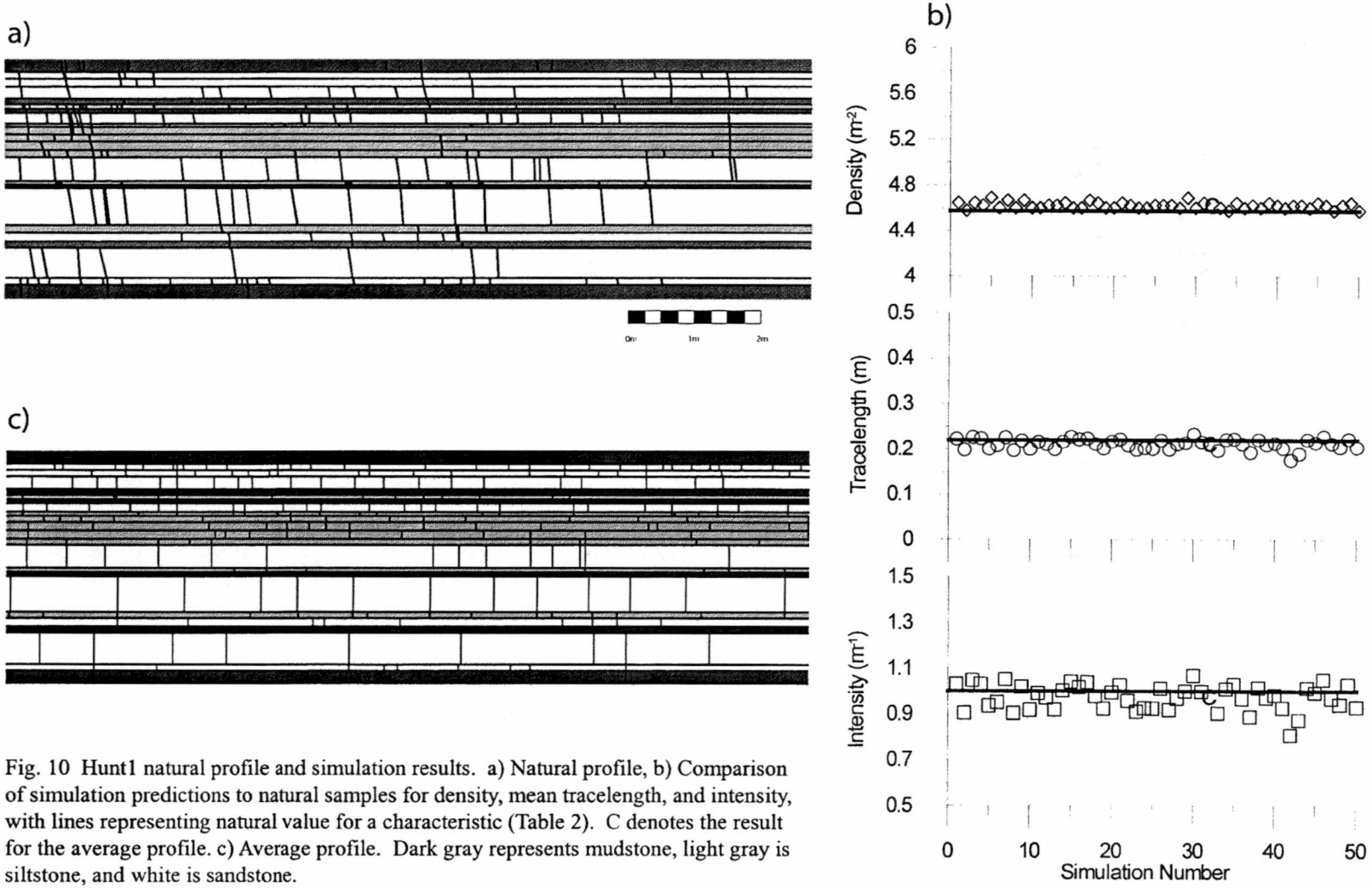


Fig. 10 Hunt1 natural profile and simulation results. a) Natural profile, b) Comparison of simulation predictions to natural samples for density, mean tracelength, and intensity, with lines representing natural value for a characteristic (Table 2). C denotes the result for the average profile. c) Average profile. Dark gray represents mudstone, light gray is siltstone, and white is sandstone.

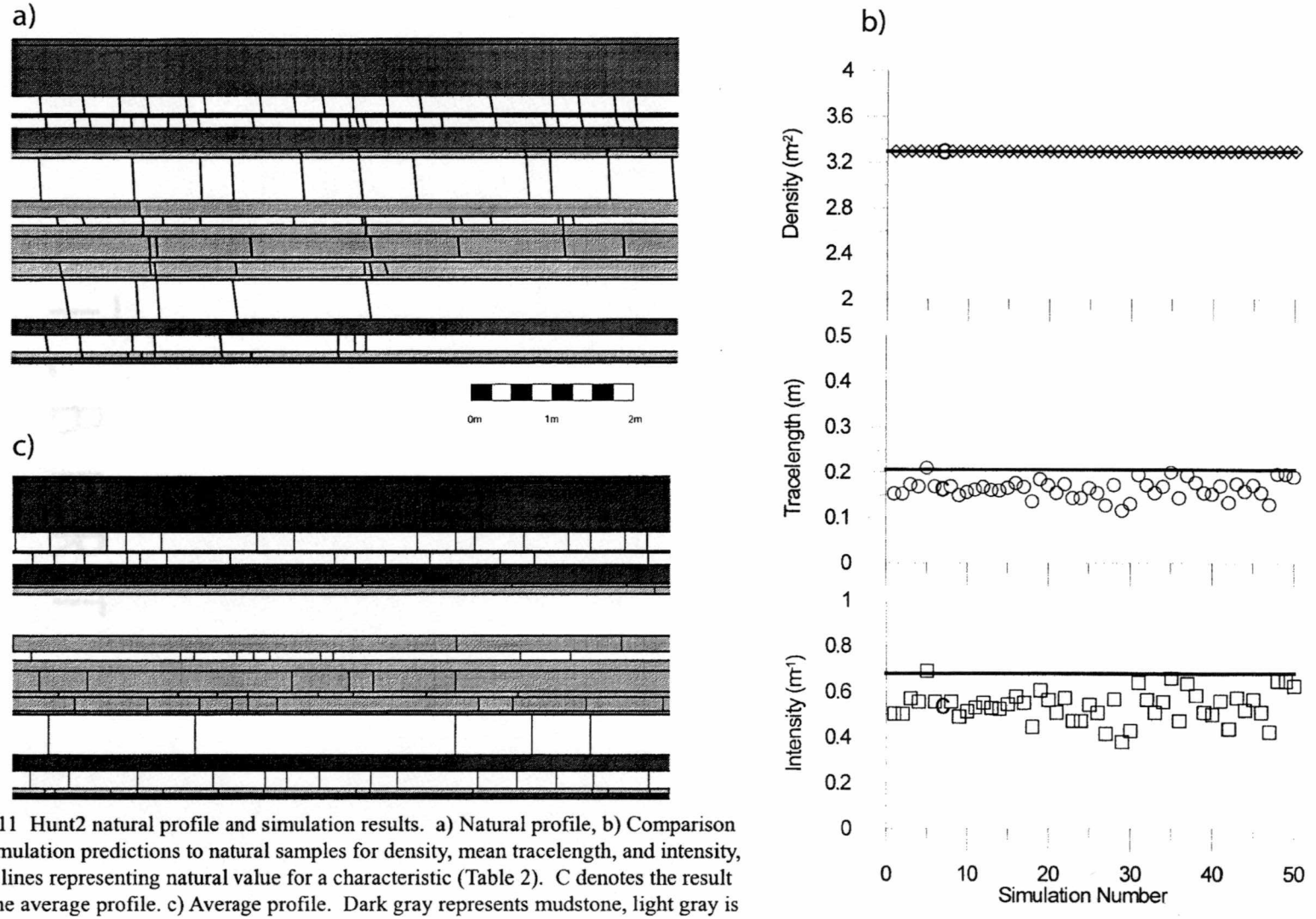
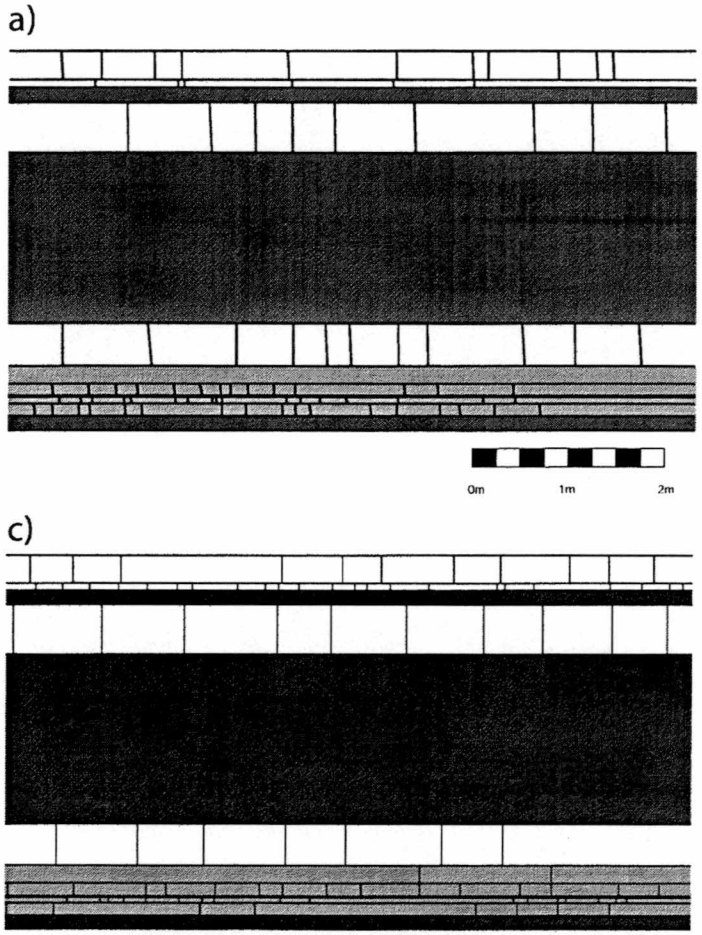


Fig. 11 Hunt2 natural profile and simulation results. a) Natural profile, b) Comparison of simulation predictions to natural samples for density, mean tracelength, and intensity, with lines representing natural value for a characteristic (Table 2). C denotes the result for the average profile. c) Average profile. Dark gray represents mudstone, light gray is siltstone, and white is sandstone.



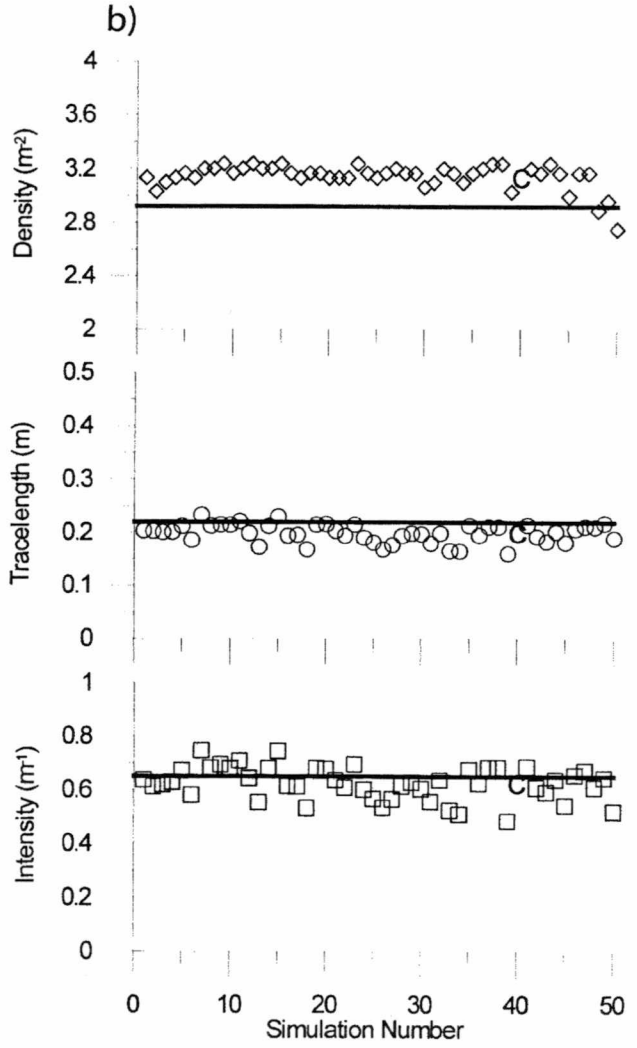


Fig. 12 Hunt3 natural profile and simulation results. a) Natural profile, b) Comparison of simulation predictions to natural samples for density, mean tracelength, and intensity, with lines representing natural value for a characteristic (Table 2). C denotes the result for the average profile. c) Average profile. Dark gray represents mudstone, light gray is siltstone, and white is sandstone.

reasonable match between the synthetic pattern and the natural pattern, their approach has three limitations. First, because the analysis matches the number of fractures on a bed-by-bed basis, the number of fractures in each bed must already be known. Thus, the methodology is only applicable to the sample area, and cannot easily be extrapolated to other areas. Second, the analysis underestimates the number of joints confined to a single bed, creating too many fractures that are not bed-contained and reducing fracture density while increasing mean tracelength for the population. This phenomenon is the result of not correlating propagation probabilities for successive beds (Pascal et al., 1997). Third, their analysis does not allow for fractures extending into or out of the sample window, creating a simulation that is artificially isolated from surrounding beds. They compensate for the lack of inward-propagating fractures by initializing extra joints inside the sample window (Pascal et al., 1997). The present analysis does not have these limitations.

5.2. Huntingdon

An outcrop of the Devonian Brallier Formation near Huntingdon, Pennsylvania (Ruf et al., 1998), provided three additional profiles. The joints in these profiles are approximately 0-10° from being bed-normal (Figs. 10-12), which may result from tilting of principal stresses by shear tractions during flexural-slip/flow folding (Engelder & Peacock, 2001). Otherwise, the joint networks exhibit typical bed-normal joint characteristics.

The Brallier Formation consists of a distal turbidite sequence of interbedded fine sandstone, siltstone, and mudstone in beds up to ~50 cm thick. Some bed-normal joints

are contained, but others cut across several beds. The oldest joint set (strike ~050°), determined by termination relationships, was the focus of this study, because fracture propagation in this set was not influenced by later fracture sets. A significant number of fractures cross one or more bedding boundaries in Hunt1 (Fig. 10a), while joints are primarily confined to single beds in Hunt2 and Hunt3 (Fig. 11a & 12a). To limit uncertainty due to incomplete exposure, the sample window was chosen to be the perimeter of the joint terminations. The effects of mechanical discontinuities, bedding boundaries and preexisting systematic fractures, on joint spacing were previously explored by Ruf et al. (1998).

5.3. Network characteristics

For each profile, pertinent bulk network characteristics of intensity, apparent density, and apparent mean tracelength were determined (Table 2). Estimations of the true density and mean tracelength were also calculated (Table 2). The density estimation is half N_T, the number of T-intersections divided by the reduced sample area. Where the reduced sample area is the sample height minus half the thickness of the top and bottom bed multiplied by the sample width. The mean tracelength estimate is the inverse of 1 over the apparent mean tracelength minus 1 over the sample window height (Mauldon, 1998)

.

For both profiles LMP and LM, some fractures extend beyond sample windows, so the mean tracelength is the apparent mean tracelength and density is the apparent density. In profile LMP, only 4 fractures extend beyond the sample window, so apparent

Table 2
Natural profile fracture pattern characteristics and simulation results

	LMP	LM	Hunt1	Hunt2	Hunt3
Natural Profile					
Intensity (m^{-1})	3.54	3.18	1.00	0.68	0.65
Density (m^{-2})	6.28	15.74	4.57	3.29	2.92
Mean Tracelength (m)	0.56	0.20	0.22	0.21	0.22
Estimated Natural Values					
Estimated Density	5.42	14.21	4.69	3.35	2.90
Estimated Mean Tracelength	0.73	0.23	0.23	0.22	0.23
Simulation Values					
Mean Intensity (m^{-1})	4.41	3.09	0.97	0.54	0.62
Simulation St. Dev.	0.84	0.07	0.06	0.07	0.06
COV (%)	19	2	6	12	10
Mean Apparent Density (m^{-2})	6.02	16.35	4.62	3.29	3.14
Simulation St. Dev.	0.28	0.19	0.03	0.00	0.09
COV (%)	5	1	1	0	3
Mean simulation Mean Tracelength (m)	0.73	0.19	0.21	0.16	0.20
Simulation St. Dev.	0.13	0.00	0.01	0.02	0.02
COV (%)	17	3	6	12	9
Comparison					
% Difference Intensity	24	3	3	21	3
% Difference Apparent Density	4	4	1	0	8
% Difference Apparent Mean Tracelength	30	6	4	21	10

density and mean tracelength are very close to the true values. For the three Huntingdon profiles (Hunt1, Hunt2, and Hunt3), all E-intersections are known to be T-intersections; therefore the apparent mean tracelength and density are also the true values.

6. Results

6.1. Simulations of ideal cases

The first step to testing this approach is to see if it generates recognizable patterns for geologically simple cases. Three simple profiles were simulated to evaluate the effects of variations in bed thickness, lithology, and bedding contact strength. The first profile (Fig. 13a) represents the case of one lithology with constant bed thickness and weak bedding contacts, so that all joints are confined to single beds. The second profile (Fig. 13b) contains a single lithology with two different bed thicknesses and strong contacts so that joints can propagate across bedding boundaries. In the third profile (Fig. 13c), the thinner beds are assigned a different lithology that prohibits joint propagation or initiation.

For simulation A, since all joints were confined to single beds by weak bedding contacts, the mean tracelength is equal to the average bed thickness (Table 3). New joints are prohibited from forming within the stress shadows of existing joints, resulting in fairly constant fracture spacing. For simulation B, joints were allowed to propagate across layer boundaries, resulting in several fractures that cross several beds. The joints, particularly in the thinner beds, still exhibit a fairly regular spacing. However, joints that are the full height of the bed have a large enough crack half-length that the reduced stress inside existing stress shadows is insufficient to prevent propagation, resulting in some fractures being closer than was possible for case A. The third simulation (C) has the largest mean tracelength because joints were confined to the thicker beds. Again, sufficiently long fractures allow some joints to propagate close to existing joints.

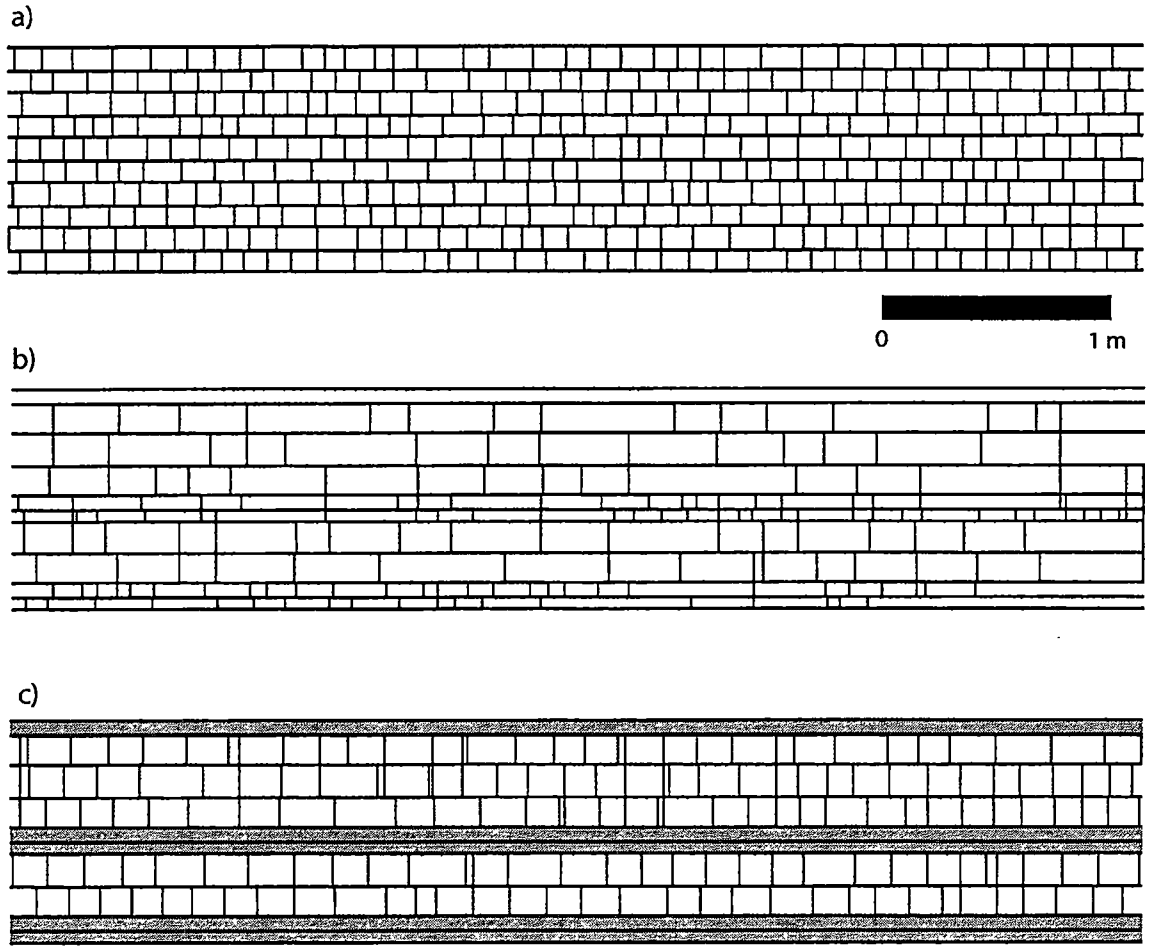


Fig. 13 Ideal case profiles. a) All beds are the same lithology and thickness (0.1 m). b) All beds are the same lithology, but now have two thickness values (0.14 m & 0.06 m). c) Same thickness values as (b), with the thinner beds being a different lithology (gray) that prevents joint initiation and propagation.

Table 3
Ideal case profile dimensions and network characteristics

	a	b	c
Window Height (m)	1	1	1
Window Length (m)	5	5	5
Window Area (m^2)	5	5	5
Number of beds	10	10	10
Number of lithologies	1	1	2
Bed Thickness 1 (m)	0.10	0.14	0.14
Bed Thickness 2 (m)	Na	0.06	0.06
Density (m-2)	78	30	30
Intensity (m-1)	7.80	3.58	4.76
Mean Tracelength (m)	0.10	0.12	0.16
T-intersections	86	85	100
X-intersections	21	18	15
E-intersections	13	14	0

Although these simulations do not represent actual joint networks, they are similar in appearance to natural fracture patterns (Gross et al., 1995; Becker & Gross, 1996; Gross et al., 1997; Pascal et al., 1997; Ruf et al., 1998). Because the program can produce reasonable ideal fracture patterns, the next step is to attempt to simulate natural joint networks.

6.2. Simulation of natural profiles

The method was tested by running simulations using data from whole profiles to yield synthetic profiles and determining if they reasonably matched the natural examples. Input data for simulations include (T, X, E) intersection counts and outcrop dimensions (Table 1), bed thicknesses and lithologies (Figs. 8a-12a), and lithology parameters (Table 4). The remote strain was chosen to yield sufficient driving stress to fracture those lithologies that contain fractures in the field (Figs. 8a-12a). Fifty simulations were run for each profile. Apparent density, apparent mean tracelength, and intensity of each simulation were compared to values for the natural profiles. It should be noted, however, that for Hunt1, Hunt2, and Hunt3, apparent field values for density and mean trace length are the best estimates of the true values, due to the lack of censoring in those examples.

Apparent trace densities in simulation profiles will exactly match the outcrop information if all fracture tips are contained within the sample window and bounding beds lack fractures as with the bounding mudstones in Hunt2 (Fig. 12a & b; Table 1, 4). The program allows fractures to propagate beyond the sample window as could happen in nature, if the appropriate lithology is adjacent to the top or bottom of the window. This

Table 4
Lithology parameters and strain for simulations

	LMP	LM	Hunt1	Hunt2	Hunt3
Limestone (K) (MPa*m^{-1})	1.25	1.25	na	na	na
Limestone (E) (MPa)	45	45	na	na	na
Sandstone (K) (MPa*m^{-1})	na	na	1.2	1.2	1.2
Sandstone (E) (MPa)	na	na	50	50	50
Siltstone (K) (MPa*m^{-1})	na	na	1	1	1
Siltstone (E) (MPa)	na	na	20	20	20
Siltstone2 (K) (MPa*m^{-1})	na	na	na	na	1
Siltstone2 (E) (MPa)	na	na	na	na	17
Mudstone (K) (MPa*m^{-1})	0.9	0.9	0.9	0.9	0.9
Mudstone (E) (MPa)	16	16	16	16	16
Strain	2.5E-04	2.5E-04	4.0E-04	4.0E-04	4.0E-04

Lithology parameters compiled from Atkinson & Meredith, 1987; Gross et al., 1996

simulated propagation may yield a different geometry than the natural profile. For example, in LM all but 4 of the 98 E-intersections are T-intersections, so any additional X-intersections, beyond 4, at the window edge of the simulation will trigger a density overestimate, which happened in all 50 simulations.

Match quality for mean tracelength is influenced by two factors: (1) which beds, thin versus thick, contain joints compared to the natural profiles; and (2) the number of fractures crossing multiple beds (Fig. 8-12; Table 1). A given bed may have a greater or fewer number of joints than the natural pattern, because the program does not match the exact number of fractures on a bed-by-bed basis. Requiring such a bed-by-bed fit would improve the match, but would destroy the predictive capability of the approach for rock volumes where fracture geometries are not known on a bed-by-bed basis. Thus, the potential for a lesser match quality is necessitated by the need to develop a predictive tool.

LM and Hunt1 produce the closest matches to the apparent mean tracelengths, with the simulation mean being within 6% for LM, and within 4% for Hunt1. The simulations for LM primarily underestimate the apparent mean tracelength, because simulated joints tended to cross one bed and not multiple beds as in the profile. Simulations for Hunt1 both under and overestimate the apparent mean tracelength, reflecting the interplay between more fractures in thin beds and fractures crossing more bedding surfaces in comparison to the natural network.

Since profiles Hunt2 and Hunt3 have very few X-intersections, fractures are primarily bed-contained, and so, the difference between simulated and natural profiles for

mean tracelength is related to the distribution of joints as a function of bed thickness. Most simulations underestimate mean tracelength, because more joints occur in thin beds in those simulations than in the natural profiles.

For the case of LMP, the simulations systematically overshoot the apparent mean tracelength, with an average 30% difference. Many simulations have significantly fewer contained joints than the natural profile, while preserving the number of T-intersections. Because this natural profile contains clustered joints (Fig. 8a) and the joints are vein filled, the fill was assumed to precipitate during fracturing, which eliminates void space and the stress shadow effect. Thus, simulations were run without the stress shadow effect. Simulated fractures can propagate more freely in the absence of stress shadows, and because longer fractures have a higher probability of being chosen to propagate they will continue to grow longer. This effect results in longer average fractures in the simulation than the natural profile.

Intensity, the product of density and mean tracelength, is the final network parameter examined (Figs. 8b-12b). LM and Hunt3 yield a very close intensity match between simulations and nature. Hunt1 also has a small density overestimation combined with small variations of mean tracelength in the simulations, which results in a good intensity match. Where a mismatch of intensity values occurs between simulations and nature, the mismatch is due to the quality of mean tracelength match because simulations produce quite close matches to natural profiles for densities. For example, Hunt2 simulations had an exact match for density, so the intensity underestimation is the result of the mean tracelength underestimation.

LMP simulations overestimated mean tracelength by an average of 30%, resulting in an overestimate of intensity in that case. Also at LMP, the simulated densities underestimated the measured apparent densities from the natural sample, and showed the largest standard deviation, at 5% of the mean. Variability in the results was greater at LMP than at the four other sites. One reason for this is that it was not possible to deduce the nature of edge-intersections at LMP, whereas at the other sites, detailed inspection allowed the assignment, in many instances, of edge-intersections to either X or T. Such additional information limited the amount of uncertainty in the sample and led to better parameter estimates and better matches between simulated pattern and field example.

Another test of the simulations is to consider if they visually resemble the natural profiles. While it is not practical to include a synthetic profile for all fifty simulations for each profile, we chose a representative example that, of the 50 simulations, most closely matched average simulation values for apparent density, apparent mean tracelength, and intensity (Figs. 8c-12c; Table 2). The values of joint characteristics for the representative profile of LM (Fig. 9) are all within 1% of the mean for the simulation population (Table 2). The simulation is a good match to the natural profile, with the only obvious difference being that the top two limestone beds have almost half the number of common joints as compared to the natural profile. For LMP, the representative profile is within 3% of the means for the simulation population (Fig. 8b). Yet, these means differ noticeably from the characteristics of the natural profile (e.g., apparent density by 5% under, apparent mean tracelength by 34% over, intensity by 27%) values for the representative simulated profile of Hunt1 differ by only 0.5% from the population means and by <4%

from the natural profile. More joints occur in the upper thin beds with less clustering in the simulation than the natural profile, but overall the visual match is good. While the apparent density match is exact for Hunt2, tracelength and intensity are <0.2% from the population mean and are 21% less than these characteristics for the natural profile. The primary cause of these effects is an overabundance of joints in the thinner beds of siltstone in the synthetic as compared to the natural profile. The overabundance of joints in siltstone beds reflects the greater number of siltstone than sandstone beds (Fig. 11). Thus, the selected lithological elastic properties are not sufficiently different to preclude joints from tracking the relative abundance of beds for the two lithologies.

For Hunt3, characteristics are within 0.5% of population means, which overestimate apparent density by 8%, and underestimate intensity and apparent mean tracelength by 3% and 10%, respectively. The tracelength underestimate is primarily an artifact of the simulation having more small fractures in thin sandstone and siltstone beds than the natural profile (Fig. 12).

At Huntingdon, the relative abundance of fractures in sandstones is not solely a function of sandstone abundance in a given natural profile. For example, Hunt2 has 73% of joints in sandstone but only 38% of the beds are sandstone, whereas Hunt3 has 44% of joints in sandstone but 57% of the beds are sandstone. Thus, unless material properties are defined for each individual bed, rather than for a given lithology, the simulations will not track the relative lithologic distributions in these different profiles using either this modeling approach or a numerical mechanical model. However, bed-by-bed characterization of properties would increase the necessary number of input parameters,

complicate data collection from the sample area, and limit the applicability of the analysis.

Overall for the five profiles, simulation characteristics are comparable to natural characteristics, and synthetic profiles appear similar to natural profiles (Fig. 9-13). Differences do occur, but would also be expected in mechanical models, and could only be eliminated by over-constraining the procedure, which would eliminate its predictive capability. Therefore, we believe that this approach does successfully simulate natural examples and can be applied to attempting to predict joint characteristics beyond a sample region.

6.3. Comparison of prediction results to natural profiles

The quality of predictions is partially a function of sample size. The five natural profiles had total X and T counts of 160 to 596, which yielded reasonable simulations of their geometry. For dealing with the case of predicting beyond a sample region, an issue is the minimum sample size necessary to provide a user with confidence in the prediction. Given this issue, we used smaller subsamples of the natural profiles to investigate the sample size necessary to reasonably predict the number of X- and T-intersections for whole profiles. Thus, for this analysis, the subsample equaled the known region and the whole natural profiles are the prediction region.

A subsample must be representative of the whole network to accurately predict the joint pattern. Wu & Pollard (1995) found that scanline samples provided a good match with area samples for well-developed (homogeneous) fracture patterns but the

quality of the match declined for poorly developed networks with greater heterogeneity. Therefore, joint network heterogeneity can greatly affect the subsample and subsequently prediction quality. The heterogeneity of the natural profiles (Fig. 8a – 12a) was examined by dividing each profile into 32 equal columns that each encompass the full outcrop height and 1/32 of the outcrop width (Table 5). The X- and T-intersections were counted for each 1/32 of a profile to determine the amount of network heterogeneity in a profile. LMP is the most homogeneous overall and LM is homogeneous for T-intersection counts. Hunt1 shows the greatest heterogeneity, with Hunt2 and Hunt3 also showing a great deal of heterogeneity for T-intersection counts. X-intersection count variations were not investigated for Hunt2 or Hunt3 because the profiles have essentially zero X-intersections, making these nearly homogeneous.

The effects of heterogeneity and sample size were explored by using independent randomly selected groups of 5, 10, 15, 20, and 25 of the 1/32 columns for a profile, with no column repetition within a group. The selection process was done 50 times for each size group, yielding a range of counts. Again, X-intersection counts for Hunt2 and Hunt3 were not considered since they are essentially zero. These counts were normalized to their respective areas and plotted against the corresponding expected X or T count (Fig. 14). Expected sample counts are determined by normalizing the whole outcrop count to the size of the subsample; for example, the ideal T-intersection count for a 5/32 sample of LM is 422 * 5/32, since the whole outcrop count is 422.

Prediction quality shows a nonlinear improvement with increasing sample size (Fig. 14). Rate of improvement in prediction quality drops noticeably in the range of 50-

Table 5
Coefficient of variation for sub-sample intersection counts

	LMP	LM	Hunt1	Hunt2	Hunt3
X-intersection count – COV	0.44	0.99	1.61	na	na
T-intersection count – COV	0.38	0.30	0.73	0.71	0.72

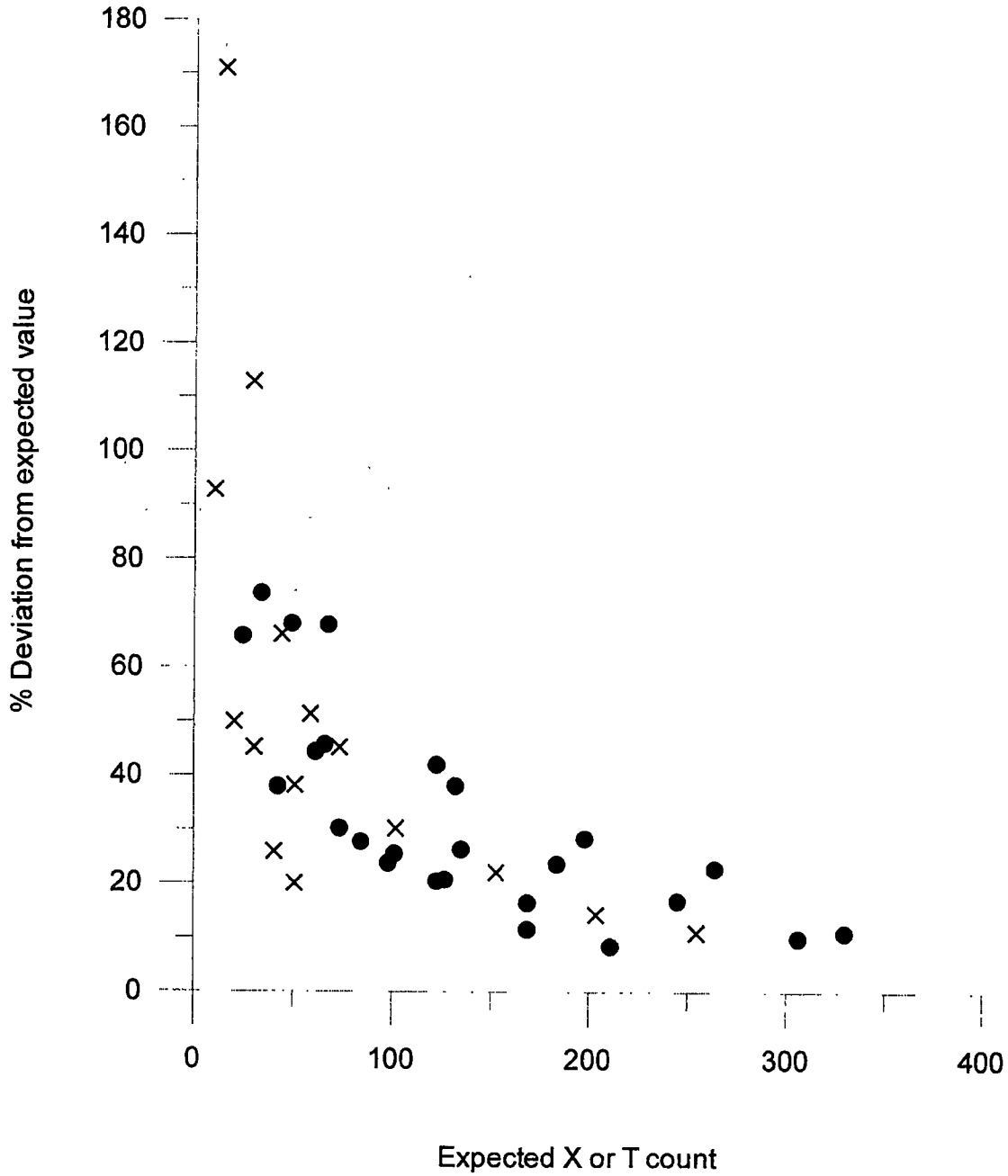


Fig. 14 Graph of % deviation from the expected count for the T-intersections for all five natural profiles and X-intersections for LMP, LM, and Hunt1, versus the normalized expected X and T counts. X's represent the X counts and cirlcles represent the T counts.

100 intersections. For 50-100 intersections, predicted counts are within 20-40% of natural values. Though these profiles are not exhaustive of all possible bed-normal joint networks, they do represent a large range of heterogeneity and bed-contained versus not bed-contained geometries. Therefore, we believe that this modeling approach is likely to limit the effects of small sample size for counts of 50-100 intersections.

7. Recommendations for future work

Though this analysis can reasonably simulate natural fracture patterns, it is limited in its scope. Some mechanical considerations were not used and some were over-simplified. Also, more detailed input information and correlations would allow for a more constrained analysis.

One phenomenon that is not considered in this model is the development of composite joints. Composite joints develop due to fractures communicating stress across bedding boundaries or thin mudstone layers (Helgeson & Aydin, 1991). To allow for composite joints, a model would need to include a function that described the amount of stress that was transmitted into a potential fracturing layer across the nonfracturing layer.

The influence of bedding contact strength during propagation is greatly simplified in this model. The program only allows the user to define contacts with certain lithologies as too weak to permit propagation. Rating types of bedding contacts as a function of lithological pairs or bedding surface geometries as strong, moderate, or weak based on field and experimental result, would allow a more complete analysis.

This analysis is limited to fractures formed by joint-normal extension, which form in nature during the extension of layered sedimentary rocks. Joint formation by thermoelastic and fluid-driving load are not considered (Engelder & Fischer, 1996). In the present analysis, eliminating the stress shadow effect may serve as a proxy for fluid-driven joints, since fluid pressure lowers the necessary driving stress (Rijken & Cooke, 2001). Also, multiple loads may contribute to joint network formation simultaneously. An improved simulation would include rules of different loads and load combinations. In

nature, multiple joints in the same set most likely form simultaneously, but this analysis is limited to forming single joints in iterative steps.

The intersection counts could also be analyzed more completely. For example, in cases where the true nature of the E-intersections is not known they could be assigned as X- or T-intersections according to the manner in which X- and T-intersections appear in the rest of the profile. Assigning E-intersections would most likely help to reduce the variability in simulation results. Secondly, it might be useful to correlate the intersection counts to the lithology with which they are associated. In addition to the overall probabilities of initiation and propagation, incremental probabilities for initiation and propagation could be calculated for each lithology, allowing the analysis to more closely match the number of fractures according to lithology. For this study, it may have improved some of the mean tracelength matches by reducing the extra joints in thin siltstone beds.

Correlating intersection counts to bed thickness might also be useful. In fracture saturated networks, joints in thin beds are typically more closely spaced than thicker beds, resulting in more fracture-bed intersections for thin beds. This geometric relationship is not necessarily true for undersaturated networks, so correlating the counts to bed thickness would allow for a more exact match. This type of correlation may reduce the difference between simulation and natural pattern mean tracelength values, but each of these detailed correlations would require more complex input data, limiting the applicability of the analysis.

8. Conclusions

(1) We present a new approach to predicting the geometry of bed-normal joints that has two key differences from previous work: combined mechanistic and probabilistic approach and considers joint-bed intersection points.

(2) Simulations using this combined approach for data from nature profiles produced a reasonable match for apparent density, apparent mean tracelength, and intensity as well as a reasonable visual similarity. Therefore, this approach can simulate and predict natural joint patterns.

(3) Joint network heterogeneity and small sample size can reduce the quality of predictions about fracture networks when applying this approach, although an intersection count of about 50-100 appears to limit this reduction.

REFERENCES CITED

Ang, A.H-S. and Tang, W.H., 1975. Probability concepts in engineering planning and design. 1. John Wiley, New York.

Atkinson, B.K., Meredith, P.G., 1987. Experimental fracture mechanics data for rocks and minerals. In: Atkinson, B.K. (Ed.), Fracture Mechanics of Rock. Academic Press, 477-525.

Bai, T., Pollard, D.D., 2000a. Fracture spacing in layered rocks a new explanation based on the stress transition. Journal of Structural Geology 22, 43-57.

Bai, T., Pollard, D.D., 2000b. Closely spaced fractures in layered rocks: initiation mechanism and propagation kinematics. Journal of Structural Geology 22, 1409-1425.

Baecher, G.B., Einstein, H.H., 1977. Statistical description of rock properties and sampling. In: Wang, Clark (Ed.). Proceedings for the 18th U.S. Symposium on Rock Mechanics, pp. 5C1.1 – 5C1.8.

Barton, C.C., 1995. Fractal analysis of scaling and spatial clustering of fractures. In: Barton, C.C., LaPointe, P.R., (Eds.). Fractals in the Earth Sciences. New York, Plenum Press, 141-178.

Barton, C.C., Larson, E., Page, W.R., Howard, T.M., 1993. Characterizing fractured rock for fluid-flow, geomechanical, and paleostress modeling: Methods and preliminary results from Yucca Mountain, Nevada. United States Geological Society Open-File Report 93-269, 62pp, 1 plate.

Becker, A., Gross, M.R., 1996. Mechanism for joint saturation in mechanically layered rocks: an example from southern Israel. Tectonophysics 257, 223-237.

Cooke, M.L., Underwood, C.A., 2001. Fracture termination and step-over at bedding interfaces due to frictional slip and interface opening. Journal of Structural Geology 23, 223-238.

Cruden, D.M., 1977. Describing the size of discontinuities. International Journal of Rock Mechanics and Mining Sciences and Geomechanical Abstracts 14, 133-137.

Dershowitz, W.S., Einstein, H.H., 1988. Characterizing rock joint geometry with joint system models. Rock Mechanics and Rock Engineering 21, 21-51.

Dershowitz, W.S., Herda, H.H., 1992. Interpretation of fracture spacing and intensity. In: Tillerson, Wawersik, (Ed.). Proceedings 33rd U.S. Symposium on Rock mechanics, Balkema, Rotterdam, pp. 19-30.

Engelder, T., 1993. Stress regimes in the lithosphere. Princeton University Press, New Jersey.

Engelder, T., Fischer, M.P., 1996. Loading configurations and driving mechanisms for joints based on the Griffith energy-balance concept. Tectonophysics 256, 253-277.

Engelder, T., Peacock, D.C., 2001. Joint development normal to regional compression during flexural-flow folding: the Lilstock buttress anticline, Somerset, England. Journal of Structural Geology 23, 259-277.

Gillespie, P.A., Walsh, J.J., Watterson, J., Bonson, C.G., Manzocchi, T., 2001. Scaling relationships of joint and vein arrays from The Burren, Co. Clare, Ireland. Journal of Structural Geology 23, 183-201.

Gross, M.R., Bahat, D., Becker, A., 1997. Relations between joint and faulting based on fracture-spacing ratios and fault-slip profiles: A new method to estimate strain in layered rocks. Geology 10, 887-890.

Gross, M.R., Engelder, T., 1991. A case for neotectonic joints along the Niagra escarpment. Tectonics 10, 631-642.

Gross, M.R., Fischer, M.P., Engelder, T., Greenfield, R.J., 1995. Factors controlling joint spacing in interbedded sedimentary rocks: integrating numerical models with field observations from the Monterey Formation, USA. In: Ameen, M.S. (ed.), Geological Society Special Publication No. 92, 215-233.

Hancock, P.L., 1985. Brittle microtectonics: principles and practice. Journal of Structural Geology 7, 437-457.

Helgeson, D.E., Aydin, A., 1991. Characteristics of joint propagation across layer interfaces in sedimentary rocks. Journal of Structural Geology 13, 897-911.

Hobbs, D., 1967. The formation of tension joints in sedimentary rocks: an explanation. Geological Magazine 104, 550-556.

Holst, T.B., Foote, G.R., 1981. Joint orientation in Devonian rocks in the northern portion of the lower peninsula of Michigan. Geological Society of America Bulletin 92, 85-93.

Huang, Q., Angelier, J., 1989. Fracture spacing and its relation to bed thickness. Geological Magazine 126, 355-362.

Hudson, J.A., Priest, S.D., 1983. Discontinuity frequency in rock masses. International Journal of Rock Mechanics and Mining Sciences and Geomechanical Abstracts 20, 73-89.

Kulatilake, P.H.S.W., 1988. Corrections for sampling biases in joint surveys; state-of-the-art. In: Fragaszy, R.J. (Ed.), Proceedings of the 24th symposium on Engineering geology and soils engineering. Boise, ID, 359-374.

LaPointe, P.R., 1993. Pattern analysis and simulation of joints for rocking engineering. In: Hudson, J.A., (Ed.). Comprehensive Rock Engineering, Volume 3 - Rock testing and site characterization, Pergamon Press, New York, pp. 215-239.

LaPointe, P.R., and Hudson, J.A., 1985. Characterization and interpretation of rock mass joint patterns. Geological Society of America Special Paper 199, 37p.

Mauldon, M., 1994. Intersection probabilities of impersistent joints. International Journal of Rock Mechanics and Mining Sciences and Geomechanical Abstracts 31, 107-115.

Mauldon, M., 1998. Estimating mean fracture trace length and density from observations in convex windows. Rock Mechanics and Rock Engineering 31, 201-216.

Mauldon, M., Dershowitz, W.S., 2000. A multi-dimensional system of fracture abundance. Geological Society of America Annual Meeting, Abstracts with Programs 32, A474.

Mauldon, M., Dunne, W.M., Rohrbaugh Jr., M.B., 2001. Circular scanlines and circular windows: new tools for characterizing the geometry of fracture traces. Journal of Structural Geology 23, 247-258.

Mauldon, M., Rohrbaugh Jr., M.B., Dunne, W.M., Lawdermilk, W., 1999. Fracture intensity estimates using circular scanlines. In: Amadei, B., et al., (Eds.), Proceedings of 37th US Rock Mechanics Symposium, Vail, CO. 2, 777-784.

Mauldon, M., Rohrbaugh Jr., M.B., Dunne, W.M., Lawdermilk, W., 1999. Mean fracture trace length and density estimators using circular windows. In: Amadei, B., et al., (Eds.), Proceedings of 37th US Rock Mechanics Symposium, Vail, CO. 2, 785-792.

McConaughy, D.T., Engelder, T., 2001. Joint initiation in bedded clastic rocks. Journal of Structural Geology 23, 203-221.

Narr, W., 1996. Estimating average fracture spacing in subsurface rock. The American Association of Petroleum Geologists Bulletin 80, 1565-1586.

Narr, W., Lerche, I., 1984. A method for estimating subsurface fracture density in core. The American Association of Petroleum Geologists Bulletin 68, 637-648.

Odling, N.E., 1997. Scaling and connectivity of joint systems in sandstones from western Norway. Journal of Structural Geology 19, 1257-1271.

Odling, N.E., Gillespie, P., Bourgine, B., Castaing, C., Chilés, J-P., Christenson, N.P., Fillion, E., Genter, A., Olsen, C., Thrane, L., Trice, R., Aarseth, E., Walsh, J.J., Watterson, J., 1999. Variations in fracture system geometry and their implications for fluid flow in fractured hydrocarbon reservoirs. Petroleum Geoscience 5, 373-384.

Olson, J.E., 1997. Natural fracture pattern characterization using a mechanically-based model constrained by geologic data – moving closer to a predictive tool. International Journal of Rock Mechanics & Mining Science 34, paper no. 237.

Olson, J., Pollard, D.D., 1989. Inferring paleostresses from natural fracture patterns: A new method. Geology, 345-348.

Pahl, P.J., 1981. Estimating the mean length of discontinuity traces. International Journal of Rock Mechanics and Mining Sciences and Geomechanical Abstracts 18, 221-228.

Parker, L.M., 1942. Regional systematic jointing in slightly deformed sedimentary rocks. Geological Society of America Bulletin 53, 381-408.

Pascal, C., Angelier, J., Cacas, M., Hancock, P.L., 1997. Distribution of joints: probabilistic modeling and case study near Cardiff (Wales, U.K.). Journal of Structural Geology 19, 1273-1284.

Pollard, D.D., Segall, P., 1987. Theoretical displacements and stresses near fractures in rock: with applications to faults, joints, veins, dikes, and solution surfaces. IN: Atkinson, B.K., (Ed). Fracture Mechanics of Rock, pp. 277-349.

Price, N.J., 1966. Fault and joint development in brittle and semi-brittle rock. Pergamon Press, New York.

Priest, S.D., 1993. Discontinuity Analysis for Rock Engineering. Chapman & Hall, New York.

Priest, S.D., Hudson, J.A., 1981. Estimation of discontinuity spacing and trace length using scanline surveys. Journal of Rock Mechanics, Mining Science and Geomechanical Abstracts 18, 183-197.

Renshaw, C.E., Pollard, D.D., 1994. Are large differential stresses required for straight fracture propagation paths? Journal of Structural Geology 16, 817-822.

Rijken, P., Cooke, M.L., 2001. Role of shale thickness on vertical connectivity of fractures: application of crack-bridging theory of the Austin Chalk, Texas. Tectonophysics 337, 117-133.

Rives, T., Razack, M., Petit, J.-P., Hencher, S.R., Lumsden, A.C., 1992. Joint spacing: analogue and numerical simulation. Journal of Structural Geology 14, 925-937.

Rohrbaugh Jr., M.B., Mauldon, M., Dunne, W.M., in review. Estimating fracture trace intensity, density and mean length using circular scanlines and circular windows. The American Association of Petroleum Geologists Bulletin.

Ruf, J.C., Kelly, A.R., Engelder, T., 1998. Investigating the effect of mechanical discontinuities on joint spacing. Tectonophysics 295, 245-257.

Segall, P., 1984. Formation and growth of extensional fracture sets. Geological Society of America Bulletin 95, 454-462.

Segall, P., Pollard, D.D., 1983. Joint formation in granitic rock of the Sierra Nevada. Geological Society of America Bulletin 94, 563-575.

Terzaghi, R.D., 1965. Sources of error in joint surveys: Geotechnique 15, 287-304.

Verbeek, E.R., Grout, M.A., 1983. Fracture history of the northern Piceance Creek Basin, Northwestern Colorado. IN: Gary, J.H., (Ed.). 16th Oil Shale Symposium Proceedings, pp. 26-44.

Warburton, P.M., 1980. A stereological interpretation of joint trace data. International Journal of Rock Mechanics and Mining Sciences and Geomechanical Abstracts 17, 181-190

Weinberger, R., 2001. Joint nucleation in layered rocks with non-uniform distribution of cavities. Journal of Structural Geology 23, 1241-1254.

Wu, H., Pollard, D.D., 1995. An experimental study of the relationship between joint spacing and layer thickness. Journal of Structural Geology 17, 887-905.

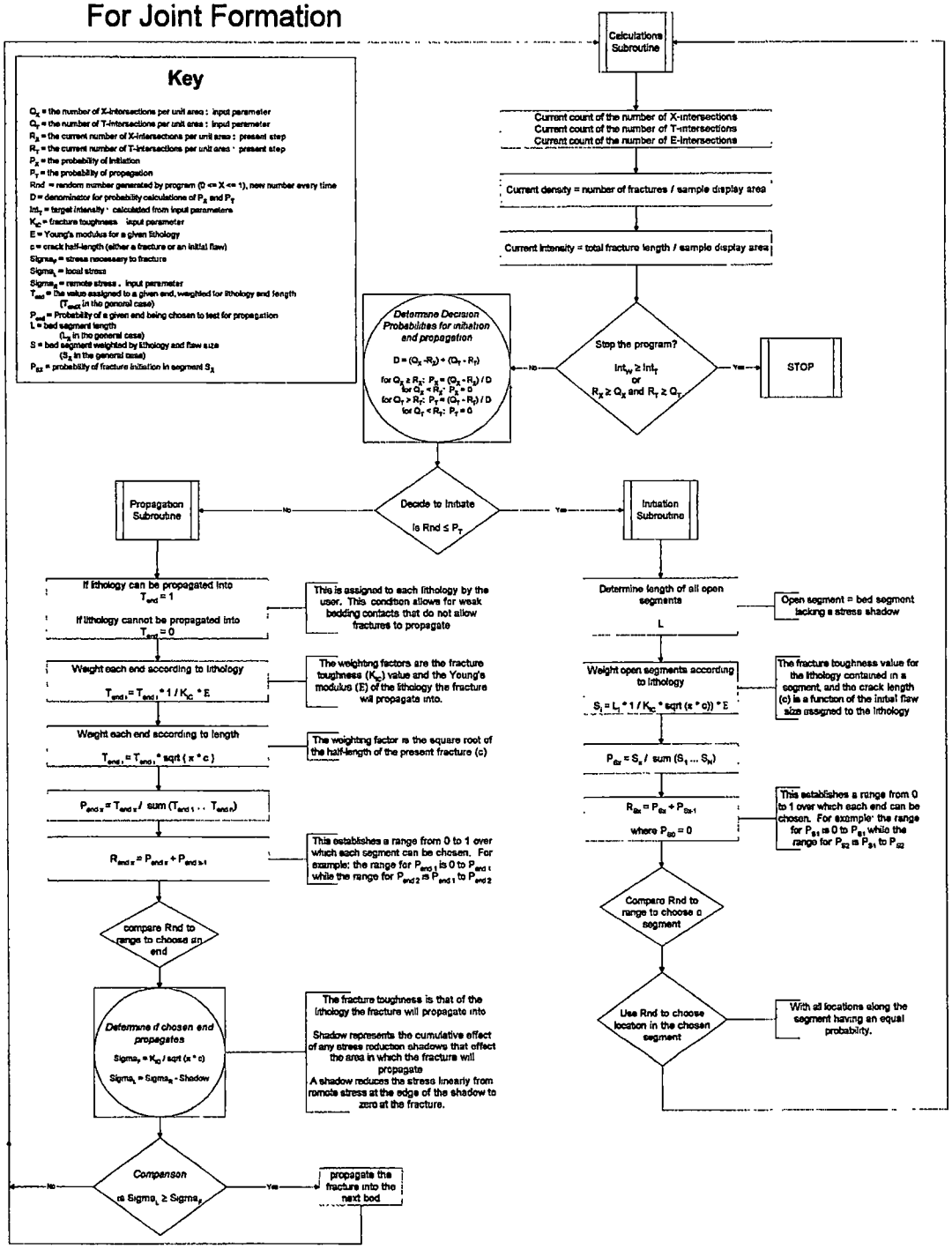
Zhang, L., Einstein, H.H., 1998. Estimating the mean trace length of rock discontinuities. Rock Mechanics and Rock Engineering 31, 217-234.

APPENDICES

Appendix A

Flow chart describing program decisions

Program Structure For Joint Formation



VITA

Wendy Faye Lawdermilk was born in Tullahoma, Tennessee on July 9, 1975. She is the daughter of Melvin and Gaye Lawdermilk. She attended Irion County High School and graduated in 1993. She then attended Texas A&M University from 1993 to 1997, where she graduated with Bachelor of Science degree in Geology. She entered the Master's program in Geology at the University of Tennessee, Knoxville in August, 1998 and focused her studies on structural geology. She officially received the Master of Science degree in December, 2001. She accepted a position with ExxonMobil, which began September, 2001.